

## MIT Open Access Articles

*Exponential Asymptotics for Line Solitons  
in Two-Dimensional Periodic Potentials*

The MIT Faculty has made this article openly available. **Please share** how this access benefits you. Your story matters.

**Citation:** Nixon, Sean D., T. R. Akylas, and Jianke Yang. "Exponential Asymptotics for Line Solitons in Two-Dimensional Periodic Potentials." *Studies in Applied Mathematics* 131, no. 2 (March 19, 2013): 149–178.

**As Published:** <http://dx.doi.org/10.1111/sapm.12006>

**Publisher:** Wiley Blackwell

**Persistent URL:** <http://hdl.handle.net/1721.1/97216>

**Version:** Author's final manuscript: final author's manuscript post peer review, without publisher's formatting or copy editing

**Terms of use:** Creative Commons Attribution-Noncommercial-Share Alike



# Exponential asymptotics for line solitons in two-dimensional periodic potentials

Sean D. Nixon<sup>1</sup>, T. R. Akylas<sup>2</sup>, and Jianke Yang<sup>1\*</sup>

<sup>1</sup> Department of Mathematics and Statistics, University of Vermont, Burlington, VT 05401, USA

<sup>2</sup> Department of Mechanical Engineering, MIT, Cambridge, MA 02139, USA

As a first step toward a fully two-dimensional asymptotic theory for the bifurcation of solitons from infinitesimal continuous waves, an analytical theory is presented for line solitons, whose envelope varies only along one direction, in general two-dimensional periodic potentials. For this two-dimensional problem, it is no longer viable to rely on a certain recurrence relation for going beyond all orders of the usual multi-scale perturbation expansion, a key step of the exponential asymptotics procedure previously used for solitons in one-dimensional problems. Instead, we propose a more direct treatment which not only overcomes the recurrence-relation limitation, but also simplifies the exponential asymptotics process. Using this modified technique, we show that line solitons with any rational line slopes bifurcate out from every Bloch-band edge; and for each rational slope, two line-soliton families exist. Furthermore, line solitons can bifurcate from interior points of Bloch bands as well, but such line solitons exist only for a couple of special line angles due to resonance with the Bloch bands. In addition, we show that a countable set of multi-line-soliton bound states can be constructed analytically. The analytical predictions are compared with numerical results for both symmetric and asymmetric potentials, and good agreement is obtained.

## 1 Introduction

Nonlinear wave propagation in periodic media is currently a subject of intensive research in optics and applied mathematics, with diverse applications ranging from nonlinear photonics [1, 2] to Bose–Einstein condensates [3, 4]. While many types of soliton structures in periodic media have been reported theoretically and experimentally (see [5] for a review), prior analytical work is limited to special (symmetric) periodic potentials [6, 7], or to one spatial dimension [8, 9, 10].

In this paper, we study line solitons in general two-dimensional periodic media, employing the nonlinear Schrödinger (NLS) equation with a spatially periodic potential as our model. Such solitons have been reported theoretically and experimentally in certain periodic potentials before [11, 12, 13, 14, 15], and it is known that they can bifurcate from edges of Bloch bands or from certain high-symmetry points inside Bloch bands. However, systematic analytical construction of line solitons is still lacking, and a number of open questions remain. It is not clear, in particular, if the inclination angles and positions of these line solitons relative to the underlying potential can be arbitrary or not.

---

\*e-mail: jyang@math.uvm.edu

To address these issues, in this article we analytically examine small-amplitude line solitons which bifurcate out from infinitesimal Bloch modes. Such solitons are in the form of slowly varying Bloch-wave packets, with the envelope of the packet being uniform along the line direction. Using standard asymptotic methods, the packet envelope can be readily shown to satisfy the familiar one-dimensional NLS equation in the absence of a potential and thus have a sech-shape. However, the position of the envelope relative to the potential is harder to determine because it hinges on effects that are exponentially small in the soliton amplitude. For this purpose, techniques of exponential asymptotics must be used.

In one-dimensional nonlinear wave systems, an exponential asymptotics method for analyzing low-amplitude solitons that comprise a periodic carrier modulated by an envelope, has been developed in the past fifteen years [8, 9, 10, 16]. This method focuses on the Fourier transform with respect to the slow spatial variable of the envelope function, motivated by the fact that the solitary-wave tails in the physical domain are controlled by the pole singularities near the real axis of the wavenumber space. The residues of these poles, which are exponentially small, are then calculated by matched asymptotics near the poles and away from the poles. The solution away from the poles, in particular, is expressed as a Taylor series of the wavenumber around zero, multiplied by a factor which is exponentially small at the poles, and the coefficients in this series are computed through a recurrence relation. Upon inverting the Fourier transform, these poles of exponentially small strength give rise to growing tails of exponentially small amplitudes in the physical solution. It turns out that these growing tails vanish only at two positions of the envelope relative to the periodic carrier, which in turn reveals that only two soliton families are admitted.

In this paper, by investigating line solitons, we present the first step in developing a fully two-dimensional asymptotic theory for the bifurcation of solitons from infinitesimal continuous waves. For line solitons, the governing equation for the carrier envelope is still one-dimensional, hence the corresponding Fourier transform depends on only one complex variable in the wavenumber domain. While this simplifies matters, two new obstacles arise. The first is that, in a two-dimensional problem, the Fourier transform of the solution contains pole singularities not only near the real axis (which we call real poles), but also away from the real axis (which we call complex poles). Which of these poles are relevant for the determination of line solitons is unclear. On this issue, we will show that it is still the real poles which matter.

The second and more serious obstacle is that, in two dimensions, the poles closest to the origin are often complex rather than real. As a consequence, utilizing a recurrence relation to determine the residues of real poles, a key step in one-dimensional problems, is no longer viable: the radius of convergence of the Taylor series (around the zero wavenumber) is limited by the nearest complex poles and thus cannot reach the real poles further away, which makes the matched asymptotics impossible to use. To overcome this obstacle, we shall give up the recurrence-relation approach and directly solve the Fourier-transformed equation along the real line of the wavenumber plane, up to the real poles. By doing so, complex poles become irrelevant and thus can be ignored. This modified approach not only turns out to be effective for two dimensions, but also simplifies the exponential asymptotics procedure: by working with the Fourier-transformed equation, the exponentially-small terms are factored out and one is left with a Volterra integral equation, which is in fact easier to solve numerically than the recurrence relation.

We apply this modified exponential asymptotics technique to line solitons bifurcating from edges of Bloch bands in general two-dimensional periodic potentials. At low amplitudes, the solution is a Bloch-wave packet whose envelope varies only in the direction normal to the line soliton. By

using the Fourier-transform approach as outlined above, we analytically calculate growing tails of exponentially small amplitudes in the normal direction. The results show that for any rational slope, two line solitons relative to the potential exist, and the positions of their envelopes can be explicitly obtained. By matching the growing and decaying tails, we also construct an infinite family of multi-line-soliton bound states. These line solitons and multi-line-soliton bound states have been obtained numerically as well, in agreement with the theory. To quantitatively verify the analytical formula for the growing tails of exponentially-small amplitude, we use this tail formula to calculate the bifurcation of the zero eigenvalue associated with the linear stability of low-amplitude line solitons. This analytical eigenvalue formula is compared with the numerical eigenvalues, and good quantitative agreement is reached. Finally, we also show that line solitons can bifurcate from interior high-symmetry points of Bloch bands as well. But such line solitons exist only for very few (up to three) special line angles due to resonance with the Bloch bands.

## 2 Line wavepackets at low amplitudes

We consider the nonlinear Schrödinger equation in two spatial dimensions with a periodic (lattice) potential,

$$i\Psi_t + \nabla^2\Psi - V(x, y)\Psi + \sigma|\Psi|^2\Psi = 0, \quad (1)$$

where  $\nabla^2 = \partial_{xx} + \partial_{yy}$ , the potential  $V(x, y)$  is periodic in both  $x$  and  $y$ , and  $\sigma = \pm 1$  is the sign of nonlinearity. This equation governs the nonlinear propagation of light in photonic lattices as well as the evolution of Bose–Einstein condensates in optical lattices [1, 2, 3, 17]. In the latter community, this equation is referred to as the Gross–Pitaevskii equation.

In this article, we shall take the minimal periods of the potential  $V(x, y)$  to be the same in both  $x$  and  $y$ . This matching periodicity in  $x$  and  $y$ , while not necessary for our analysis, allows for simplification of the algebra. For a periodic potential with matching periodicity, rotation by an angle  $\theta$ , with  $\tan(\theta)$  rational, also yields a periodic potential, but the periods of the new potential would change in general. For instance, for the potential  $V(x, y) = \sin^2 x + \sin^2 y$  with matching periods  $\pi$ , a  $45^\circ$ -rotation would yield a potential with matching periods  $\sqrt{2}\pi$ . To remove this rotational freedom and the changing periods of the same potential, we align the potential in such a way that its periods are minimal. We call the potential in such orientation as the minimal-period-orientation potential, and this potential is used throughout the paper. Without loss of generality, we also normalize the matching periods of this minimal-period-orientation potential as  $\pi$ .

We search for stationary solutions to Eq. (1) of the form

$$\Psi(x, y, t) = \psi(x, y)e^{-i\mu t}, \quad (2)$$

where  $\mu$  is the propagation constant and  $\psi$  is a real-valued amplitude function that satisfies the equation

$$\nabla^2\psi + (\mu - V(x, y))\psi + \sigma\psi^3 = 0. \quad (3)$$

In this article, we shall consider line-soliton solutions that are bounded (non-decaying) along a certain line in the  $(x, y)$  plane but decay to zero along the direction orthogonal to this line. These solutions may bifurcate out from edges of Bloch bands, or from certain high-symmetry points inside Bloch bands [12, 13, 14, 15]. Our analysis will be developed first for line solitons bifurcating from edges of Bloch bands. Afterwards (in section 11) we shall consider line solitons bifurcating from

interior points of the Bloch bands, which do exist but under more restrictive conditions due to resonance with Bloch bands.

Near edges of Bloch bands, solitons are low-amplitude wavepackets comprising the underlying Bloch-wave carrier modulated by a slowly varying envelope, and they can be studied using multiple-scale perturbation theory. For line solitons, the envelope only varies in one direction and the associated ‘slow’ spatial variable will be

$$W = \epsilon w, \quad w \equiv x \sin \theta - y \cos \theta, \quad (4)$$

where  $\theta$  is the angle the line soliton makes with the  $x$  axis, and  $\sqrt{|\mu - \mu_0|} = \epsilon \ll 1$  is the deviation from the edge point  $\mu_0$ . Plugging this into equation (3) yields

$$L_0\psi + \epsilon\partial_W L_1\psi + \epsilon^2\partial_W^2\psi + \sigma\psi^3 + (\mu - \mu_0)\psi = 0, \quad (5)$$

where

$$L_0 = \nabla^2 + \mu_0 - V(x, y), \quad L_1 = 2\nabla \cdot [\sin \theta, -\cos \theta]. \quad (6)$$

The perturbation series solution to Eq. (5) is readily found to be

$$\psi(x, y, W) = \epsilon A(W)b(x, y) + \epsilon^2 A'(W)\nu(x, y) + O(\epsilon^3), \quad (7)$$

where the functions of the fast variables satisfy

$$L_0 b(x, y) = 0, \quad (8)$$

$$L_0 \nu(x, y) = -L_1 b(x, y). \quad (9)$$

Eq. (8) implies that  $b(x, y)$  is a Bloch mode at the edge point  $\mu = \mu_0$ . For simplicity of the analysis, we shall make the following assumption.

**Assumption 1** The Bloch mode at the band edge  $\mu = \mu_0$  is unique (up to a multiplication constant).

This assumption is for the purpose of avoiding nonlinear interactions between different Bloch modes at the same band-edge point, and it holds for many band edges. We also normalize  $b(x, y)$  so that  $\max|b| = 1$ .

The inhomogeneous equation (9) is solvable, since the right-hand side  $-L_1 b$  is clearly orthogonal to the homogeneous solution  $b(x, y)$  so the Fredholm condition is satisfied. To avoid ambiguity of the homogeneous term in  $\nu$ , we require  $\langle \nu, b \rangle = 0$ , where the inner product is defined as

$$\langle f, g \rangle = \int_0^{2\pi} \int_0^{2\pi} f^*(x, y)g(x, y) \, dx dy, \quad (10)$$

with the superscript ‘\*’ representing complex conjugation.

From the solvability condition at order  $\epsilon^3$ , the envelope function  $A(W)$  in expansion (7) satisfies

$$DA'' + \eta A + \sigma a A^3 = 0, \quad (11)$$

with

$$D = \frac{\langle L_1 \nu + b, b \rangle}{\langle b, b \rangle}, \quad \eta = \text{sgn}(\mu - \mu_0), \quad a = \frac{\langle b^3, b \rangle}{\langle b, b \rangle}. \quad (12)$$

When  $\text{sgn}(\sigma) = \text{sgn}(D) = -\text{sgn}(\eta)$ , the solution of the envelope equation (11) is

$$A(W) = \alpha \operatorname{sech} \frac{W - W_0}{\beta}, \quad (13)$$

where  $W = W_0$  is the center position of the line envelope, and

$$\alpha = \sqrt{2/a}, \quad \beta = \sqrt{|D|}. \quad (14)$$

The asymptotic expansion (7) may be carried to all powers of  $\epsilon$ , with all terms being localized in  $W$  (i.e., localized along the normal direction of the line solution), suggesting that line solitons exist for all choices of  $W_0$ . However, based on previous experience and numerical computations, this is not the case. Specifically, it turns out that for rational  $\tan \theta$ , only two line-soliton families exist (not counting their periodic replications in the lattice). These two soliton families are illustrated in Fig. 1 for  $\sigma = 1$ ,  $\epsilon = 0.25$  and  $\tan \theta = 1, 2$  in the specific lattice

$$V(x, y) = 6 (\sin^2 x + \sin^2 y), \quad (15)$$

where they bifurcate out from the lowest Bloch-band edge  $\mu_0 = 4.1264$ . Solitons in the upper panels have  $W_0 = 0$  and are called onsite solitons, while those in the lower panels have  $W_0 = \epsilon\pi/2$  and are called offsite solitons.

This discrepancy between the prediction of the multi-scale expansion (7) and true solutions was first studied in [18] for a one-dimensional problem, and it was suggested that the issue could be resolved by requiring that a Melnikov-integral condition be satisfied by the leading-order approximation of (7). While this constraint happens to specify  $W_0$  correctly for symmetric potentials, in a general lattice all terms in the perturbation expansion (7) make contributions to the Melnikov integral at the same order of  $\epsilon$ , and the calculations involved quickly get out of hand. To handle this difficulty, an exponential-asymptotics approach was developed for one-dimensional problems in [8, 10], following an earlier treatment of a similar problem in the fifth-order KdV equation [16]. In the next sections, we shall adapt this exponential-asymptotics method to the study of line solitons. For this two-dimensional problem, certain key steps in the previous exponential-asymptotics procedure are no longer viable, and suitable modifications will be needed in order to overcome those obstacles.

### 3 Solution in the wavenumber domain

The failure of the multi-scale expansion (7) stems from the fact that, for generic values of the envelope position  $W_0$ , the exact solution  $\psi(x, y; W)$  contains growing tails when  $W \ll -1$  or  $W \gg 1$ ; but the amplitudes of these tails are exponentially small in  $\epsilon$ , and hence invisible in the expansion (7). In order to obtain true line solitons, we shall first calculate these exponentially small growing tails and then determine the envelope position  $W_0$  by insisting that these tails vanish.

As before [8, 10, 16], we shall work in the wavenumber domain. First, we take the Fourier transform of  $\psi(x, y, W)$  with respect to the slow variable  $W$ ,

$$\widehat{\psi}(x, y, K) = \frac{1}{2\pi} \int_{-\infty}^{\infty} \psi(x, y, W) e^{-iKW} dW. \quad (16)$$

Under this transformation, the growing tails of exponentially small amplitude in  $\psi(x, y, W)$  are transformed into poles of  $\widehat{\psi}$  with exponentially small residues.

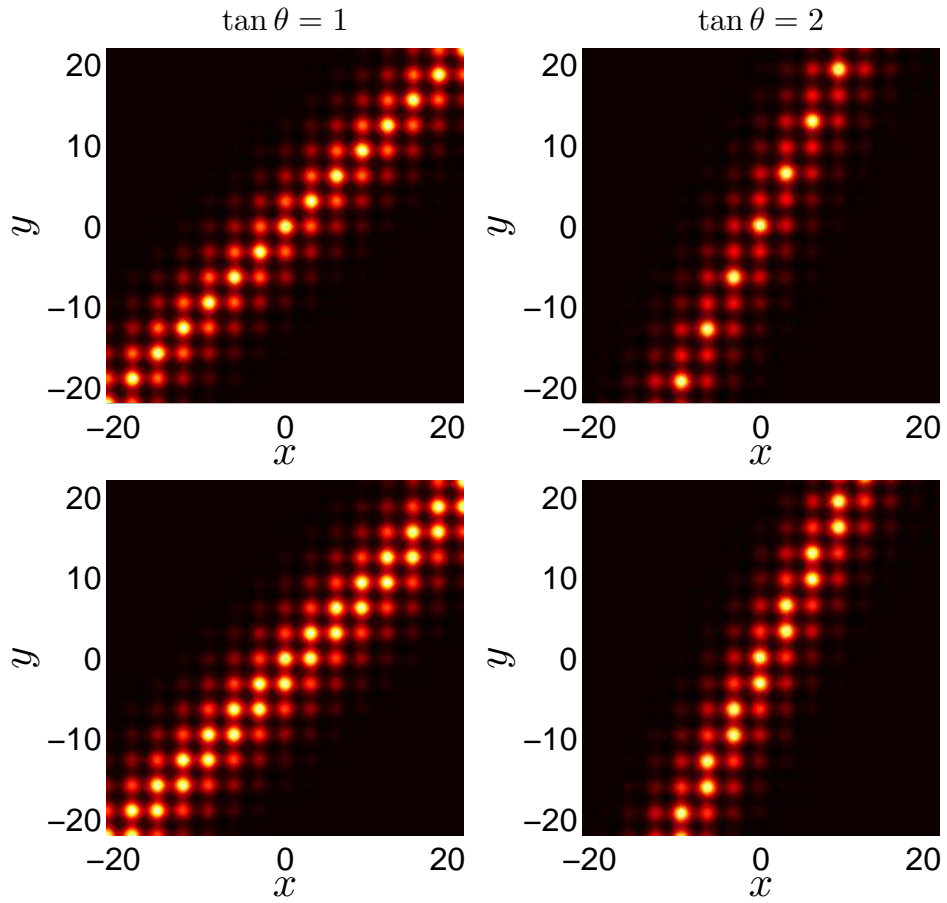


Figure 1: (Color online) Line solitons for  $\sigma = 1$ ,  $\epsilon = 0.25$  and  $\tan \theta = 1, 2$  in the lattice (15). Upper row: onsite solitons; lower row: offsite solitons.

Taking the Fourier transform of the series solution (7) term-by-term yields

$$\widehat{\psi}(x, y, K) = \epsilon \frac{\alpha\beta}{2} e^{-iW_0 K} \operatorname{sech}\left(\frac{\pi\beta K}{2}\right) \{b(x, y) + i\epsilon K\nu(x, y) + \dots\}. \quad (17)$$

This series is disordered at  $\epsilon K \sim 1$ . Thus, we introduce the ‘slow’ wavenumber  $\kappa = \epsilon K$  and rearrange this series as

$$\widehat{\psi}(x, y, \kappa) = \epsilon e^{-iW_0 \kappa / \epsilon} \operatorname{sech}\left(\frac{\pi\beta\kappa}{2\epsilon}\right) U(x, y, \kappa; \epsilon), \quad (18)$$

where

$$U(x, y, \kappa; \epsilon) = \frac{\alpha\beta}{2} \{b(x, y) + i\kappa\nu(x, y) + \dots\}, \quad \kappa \ll 1. \quad (19)$$

We now derive the governing equation for  $U$  by taking the Fourier transform of equation (3) to arrive at

$$L_0 \widehat{\psi} + i\kappa L_1 \widehat{\psi} - \kappa^2 \widehat{\psi} + \sigma \widehat{\psi}^3 + \epsilon^2 \eta \widehat{\psi} = 0. \quad (20)$$

Then, by substituting the expression (18), we find that  $U$  satisfies

$$L_0 U + i\kappa L_1 U + (\eta\epsilon^2 - \kappa^2)U + \sigma \cosh\left(\frac{\pi\beta\kappa}{2\epsilon}\right) \times \int_{-\infty}^{\infty} \int_{-\infty}^{\infty} \frac{U(\kappa - r)U(r - s)U(s)}{\cosh\left(\frac{\pi\beta(\kappa - r)}{2\epsilon}\right) \cosh\left(\frac{\pi\beta(r - s)}{2\epsilon}\right) \cosh\left(\frac{\pi\beta s}{2\epsilon}\right)} dr ds = 0. \quad (21)$$

## 4 Poles in the wavenumber plane

We are concerned with pole singularities in  $U(x, y, \kappa; \epsilon)$  which account for the growing tails in the physical space. Singularities of  $U$  are expected to occur near values of  $\kappa = \kappa_0$  where the linear part of equation (21) is zero, i.e.,

$$L_0 \phi + i\kappa_0 L_1 \phi - \kappa_0^2 \phi = 0. \quad (22)$$

With a change of variables  $\phi = e^{-i\kappa_0 w} \widetilde{\phi}$ , where  $w$  is defined in Eq. (4), equation (22) reduces to

$$L_0 \widetilde{\phi} = 0, \quad (23)$$

which has a single bounded solution  $\widetilde{\phi} = b(x, y)$ , the Bloch mode at band edge  $\mu_0$ . Thus, if we restrict ourselves for the moment to real values of  $\kappa_0$ , bounded solutions to Eq. (22) are

$$\phi(x, y) = e^{-i\kappa_0 w} b(x, y). \quad (24)$$

Since the spatial period of the solution  $\phi(x, y)$  should match that of the solution (19),  $\phi(x, y)$  and  $b(x, y)$  should have the same periodicity in  $(x, y)$ . Then following the argument in [8], both  $\kappa_0 \cos(\theta)$  and  $\kappa_0 \sin(\theta)$  should be even integers. For this to occur,  $\tan \theta$  must be a rational number, say

$$\tan(\theta) = p/q, \quad (25)$$

where  $p$  and  $q$  are relatively prime. Now to satisfy the periodicity condition, we get

$$\kappa_0 = 2n\sqrt{p^2 + q^2} \quad (26)$$

for any integer  $n$ . Thus poles of  $U(x, y, \kappa; \epsilon)$  near the real axis of  $\kappa$  are located near these  $\kappa_0$  values.

To get the approximate locations of all poles in  $U(x, y, \kappa; \epsilon)$ , we repose Eq. (22) as an eigenvalue problem

$$i \begin{bmatrix} L_1 & L_0 \\ -1 & 0 \end{bmatrix} \vec{\phi} = \kappa_0 \vec{\phi}, \quad (27)$$

where  $\vec{\phi} = [\phi, (1/i\kappa_0)\phi]^T$ , with the superscript ‘ $T$ ’ denoting vector transpose. It can be easily shown that all eigenvalues in (27) come in quadruples  $(\kappa_0, -\kappa_0, \kappa_0^*, -\kappa_0^*)$ . This spectrum also has periodicity  $2\sqrt{p^2 + q^2}$  in the real direction of  $\kappa_0$ .

Numerically we solve the eigenvalue problem (27) using the Fourier collocation method to get rough estimates of the spectrum, followed by the Newton-conjugate-gradient method to calculate particular eigenvalues to high accuracy [5]. Examples of this spectrum are shown in Fig. 2 for the lattice (15) at  $\mu_0 = 4.1264$  (the edge of the semi-infinite gap) and  $\tan \theta = 1, 2$ . Notice that this spectrum contains not only the real eigenvalues given by Eq. (26), but also a large number of complex eigenvalues. In addition, when  $\tan \theta \neq 0$ , the eigenvalues closest to the origin are complex eigenvalues rather than real eigenvalues.

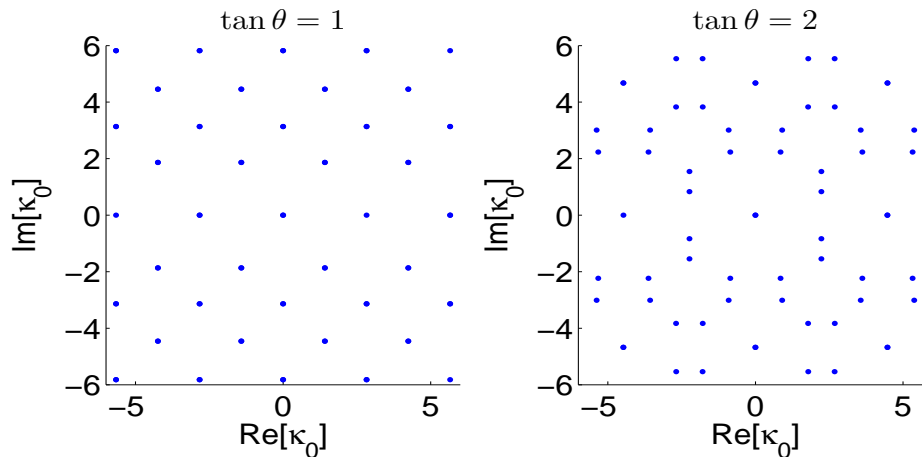


Figure 2: Locations of singularities in the wavenumber domain for the lattice (15) with  $\tan \theta = 1, 2$ .

The spectra in Fig. 2 raise serious questions on the applicability of the exponential-asymptotics method, as used earlier for solitons in one-dimensional lattices, to this two-dimensional problem. We recall that, in the one-dimensional case [8, 10, 16], this spectrum contains only real eigenvalues; and it is those real eigenvalues which specify the envelope positions. In the present case, where both real and complex eigenvalues exist, which of those eigenvalues are responsible for selecting the envelope positions?

To tackle this issue, we consider line solitons in a simpler stripe lattice, where the lattice varies in the  $x$ -direction only. The particulars of the analysis are covered in the appendix. For such a lattice, we find that the spectrum contains only complex eigenvalues and no nonzero real eigenvalues. Here, however, the envelope position of a line soliton can be arbitrary, as solutions with different envelope positions are equivalent to each other under a vertical translation. This indicates that the envelope position is not affected by complex eigenvalues, and thus we shall focus on poles of  $U(x, y, \kappa; \epsilon)$

near the real eigenvalues (26). In particular, we need to determine the residues of poles near the smallest real eigenvalues

$$\kappa_0 = \pm 2\sqrt{p^2 + q^2}, \quad (28)$$

since those poles provide the dominant contributions to the solitary-wave tails.

Even though only real eigenvalues affect the envelope position, the fact that the eigenvalues closest to the origin are complex rather than real, as shown in Fig. 2, poses a major obstacle to the calculation of the residues of poles near the real eigenvalues  $\kappa_0 = \pm 2\sqrt{p^2 + q^2}$  by the previous exponential-asymptotics technique [8, 10, 16]. This difficulty and its resolution will be elaborated in the next section.

## 5 Solution away from the poles

The basic idea for calculating the residues of poles in  $U(x, y, \kappa; \epsilon)$  is to match the ‘inner’ solution near the poles to the ‘outer’ solution away from the poles. Since the poles of interest are near  $\kappa_0 = \pm 2\sqrt{p^2 + q^2}$ , in this section we will determine the solution  $U(x, y, \kappa; \epsilon)$  for real values of  $\kappa$  in the interval  $-\kappa_0 < \kappa < \kappa_0$  but not close to  $\pm\kappa_0$ .

When  $\epsilon \rightarrow 0$ , the main contribution of the double integral in (21) comes from the triangular region  $0 < s < \kappa$ ,  $0 < s < r$  when  $\kappa > 0$  or  $\kappa < s < 0$ ,  $r < s < 0$  when  $\kappa < 0$ . Over this region,

$$\cosh\left(\frac{\pi\beta\kappa}{2\epsilon}\right) \Big/ \left[ \cosh\left(\frac{\pi\beta(\kappa-r)}{2\epsilon}\right) \cosh\left(\frac{\pi\beta(r-s)}{2\epsilon}\right) \cosh\left(\frac{\pi\beta s}{2\epsilon}\right) \right] \approx 4, \quad (29)$$

while outside this region the same expression is exponentially small. Thus, to  $O(\epsilon^2)$  the integral equation (21) reduces to the ‘‘outer’’ equation

$$\begin{aligned} L_0 U^{(0)} + i\kappa L_1 U^{(0)} - \kappa^2 U^{(0)} \\ + 4\sigma \int_0^\kappa dr U^{(0)}(x, y, \kappa - r) \int_0^r ds U^{(0)}(x, y, r - s) U^{(0)}(x, y, s) = 0, \end{aligned} \quad (30)$$

where  $U(x, y, \kappa; \epsilon) = U^{(0)}(x, y, \kappa) + O(\epsilon^2)$ . Here the main contribution to the error of the integral comes from the three corners of the triangular integration region in the integral of (30); thus this error is  $O(\epsilon^2)$ , a result that has also been checked numerically for randomly chosen analytic functions of  $U(\kappa)$ .

In previous applications of exponential asymptotics, this outer integral equation was solved by expanding  $U^{(0)}(x, y, \kappa)$  into a power series of  $\kappa$ , which turns the outer integral equation into a recurrence relation for the coefficients of the power series [8, 10, 16]. This treatment was possible since the poles of interest were closest to the origin, hence the power series was convergent up to those poles. In the present two-dimensional problem, however, this treatment fails, because the power series for  $U^{(0)}(x, y, \kappa)$  has radius of convergence bounded by the distance to the nearest complex poles. Thus this power series cannot converge near the real poles of interest. As a result, the previous approach of relying on the recurrence relation needs to be abandoned.

Instead, we propose to solve the outer integral equation (30) numerically. Since this is a Volterra integral equation, it can be easily tackled by explicit numerical methods. First we discretize  $\kappa$ ,  $\kappa_n = n\Delta\kappa$ , and write

$$U^{(0)}(x, y, \kappa_n) = U_n(x, y). \quad (31)$$

Then we approximate the integral in (30) using the trapezoid rule. After the terms in the resulting equation are rearranged,  $U_n$  is found to satisfy a linear inhomogeneous equation

$$[L_0 + i\kappa_n L_1 - \kappa_n^2 + 2\sigma U_0^2(\Delta\kappa)^2] U_n = -4\sigma F_n, \quad (32)$$

where the inhomogeneous term  $F_n$  is given by

$$F_n = \Delta\kappa^2 \left[ \frac{1}{2} U_0 I_n + \sum_{m=1}^{n-1} U_m I_{n-m} \right], \quad (33a)$$

$$I_m = \sum_{l=0}^{m-1} U_l U_{m-l}, \quad \text{for } 1 \leq m < n, \quad (33b)$$

$$I_n = \sum_{l=1}^{n-1} U_l U_{n-l}. \quad (33c)$$

Since the inner sums  $I_m$  for  $m < n$  do not change on further iterations, these only need to be computed once. Notice that the homogeneous operator in Eq. (32) is self-adjoint, thus this linear inhomogeneous equation can be solved by the preconditioned conjugate gradient method. The initial conditions  $U_0$  and  $U_1$  cannot be derived from Eq. (32) itself, but they can be obtained from the equation (19) as

$$U_0(x, y) = \frac{\alpha\beta}{2} b(x, y), \quad U_1(x, y) = \frac{\alpha\beta}{2} [b(x, y) + i\Delta\kappa \nu(x, y)]. \quad (34)$$

The above numerical scheme for solving the outer integral equation (30) is explicit. Our numerical testing shows that its numerical error is  $O(\Delta\kappa)$ , thus it is first order accurate in  $\Delta\kappa$ . If one wishes for a higher-order numerical scheme, then instead of the trapezoidal rule, one can use a higher-order quadrature method (such as Simpson's rule) to approximate the integral in (30).

From the local analysis near the poles in the next section, it will transpire that  $U^{(0)}(x, y, \kappa)$  has a fourth-order pole at  $\kappa_0$ . Specifically,

$$U^{(0)}(x, y, \kappa) \rightarrow \frac{12C}{5} \frac{b(x, y)}{(\kappa - \kappa_0)^4} e^{-i\kappa_0 w}, \quad \text{as } \kappa \rightarrow \kappa_0, \quad (35)$$

where  $C$  is a complex constant. With a change of variables

$$\tilde{U}(x, y, \kappa) = (\kappa - \kappa_0)^4 U^{(0)}(x, y, \kappa), \quad (36)$$

then

$$\tilde{U}(x, y, \kappa) \rightarrow \frac{12C}{5} b(x, y) e^{-i\kappa_0 w}, \quad \text{as } \kappa \rightarrow \kappa_0. \quad (37)$$

Numerically we have confirmed the above outer-solution behavior near the poles. As an example, the numerical results for the lattice (15) with  $\sigma = 1$ ,  $\tan \theta = 1$  and  $\mu_0 = 4.1264$  (edge of the semi-infinite gap) are shown in figure 3. For this line slope,  $\kappa_0 = 2\sqrt{2}$ . On the top left the contour plots of  $\tilde{U}(x, y, \kappa_0)$  are displayed. The corresponding analytic formula (37) with real  $C$  is also shown at the bottom for comparison. One can see that the two solutions match very well. On the right side of Fig. 3, the solution  $\tilde{U}(0, 0, \kappa)$  is shown. When  $\kappa \rightarrow \kappa_0$ ,  $\tilde{U}(0, 0, \kappa) \rightarrow 22.05$ , thus the fourth-order pole at  $\kappa = \kappa_0$  is numerically confirmed. If  $\tan \theta = 2$ , then we find that  $\tilde{U}(0, 0, \kappa) \rightarrow 4.04 \times 10^4$  as

$\kappa \rightarrow \kappa_0 = 2\sqrt{5}$ . Recalling the analytical formula (37) and Bloch-mode normalization (which boils down to  $b(0, 0) = 1$  here), the constant  $C$  is then inferred as

$$C = 9.19, \quad \text{for } \tan \theta = 1, \quad (38)$$

$$C = 1.68 \times 10^4, \quad \text{for } \tan \theta = 2. \quad (39)$$

In section 9 we are able to verify these values of  $C$  quantitatively, by comparing our predictions to numerical calculations of a certain linear-stability eigenvalue.

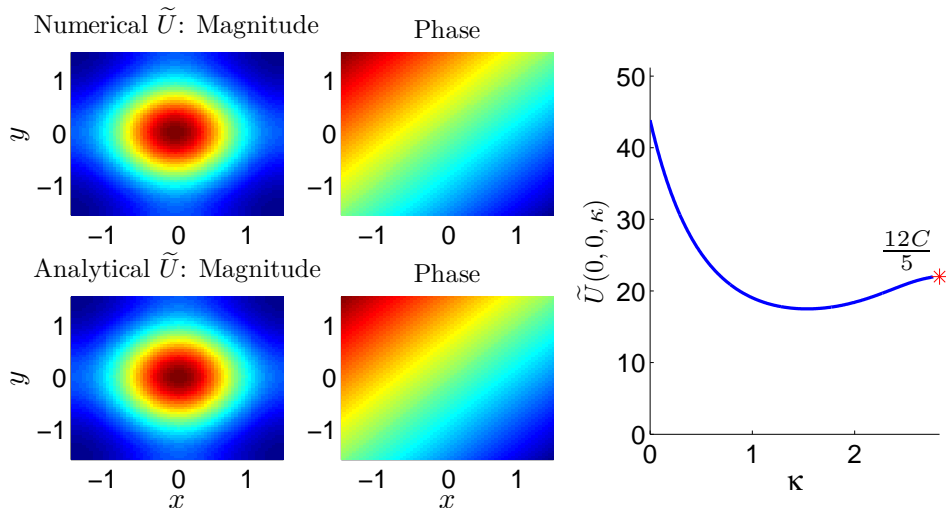


Figure 3: (Color online) Numerical solutions of the outer integral equation (30) for the lattice (15) with  $\sigma = 1$  and  $\tan \theta = 1$ . Left panels: solutions at the singularity  $\kappa = \kappa_0$ ; upper row: the numerical solution, lower row: the analytical solution. Right panel: the solution versus  $\kappa$  at  $x = y = 0$ .

The approach taken here of directly solving the outer integral equation (30) by numerical methods not only overcomes the inadequacy of the recurrence relation (for two-dimensional problems), but also has a number of additional advantages. Specifically, compared with the computation of recurrence relations in earlier works [8, 10, 16], the direct numerical solution of the outer integral equation, as was explained above, is actually easier. In addition, this direct computation gives directly the pole strength (35) in the outer solution, while in the previous approach the pole strength was inferred indirectly from the recurrence solution. In view of these advantages, it is concluded that this direct solving of the outer integral equation also simplifies the exponential asymptotics procedure.

## 6 Solution near the poles

Based on experience from prior work [8, 10, 16], the actual poles in the solution  $U(x, y, \kappa; \epsilon)$  are expected to be  $O(\epsilon)$  away from the real axis. To determine the residues of these true poles, we need to analyze the solution  $U(x, y, \kappa; \epsilon)$  near these poles. In this ‘inner’ region, the reduced outer equation (30) does not hold, and one needs to work with the full equation (21) instead. For line

solitons, it turns out that the analysis of the inner solution nearly replicates that in earlier works [8, 10, 16], thus we shall keep this discussion brief.

Focusing on the behavior of the solution  $U(x, y, \kappa; \epsilon)$  in the inner region near the closest positive singularity,

$$\kappa_0 = 2\sqrt{p^2 + q^2}, \quad (40)$$

we introduce an inner variable,  $\xi = (\kappa - \kappa_0)/\epsilon$ , that is  $\kappa = \kappa_0 + \epsilon\xi$ , with  $\xi = O(1)$ . In this region we expand the solution to integral equation (21) as

$$U(x, y, \kappa; \epsilon) = \frac{e^{-i\kappa_0 w}}{\epsilon^4} \left\{ \Phi_0(\xi)b(x, y) + i\epsilon\xi\Phi_0(\xi)\nu(x, y) + O(\epsilon^2) \right\}. \quad (41)$$

Here the order of the solution near the pole  $U = O(\epsilon^{-4})$  is chosen to match the large- $\xi$  behavior of the solution  $\Phi_0(\xi) = O(\xi^{-4})$  (see Eq. (54) below).

The dominant contribution from the double integral in equation (21) comes from the three regions: (i)  $r \approx 0$ ,  $s \approx 0$ , (ii)  $r \approx \kappa$ ,  $s \approx 0$ , and (iii)  $r \approx \kappa$ ,  $s \approx \kappa$ . In the first region,

$$U(x, y, r - s) \approx U(x, y, s) \approx \frac{\alpha\beta}{2}b(x, y), \quad (42)$$

$$U(x, y, \kappa - r) \approx \frac{e^{-i\kappa_0 w}}{\epsilon^4} \Phi_0\left(\frac{\kappa - \kappa_0 - r}{\epsilon}\right)b(x, y), \quad (43)$$

$$\cosh \frac{\pi\beta\kappa}{2\epsilon} \Big/ \cosh \frac{\pi\beta(\kappa - r)}{2\epsilon} \approx e^{\pi\beta r/2\epsilon}. \quad (44)$$

Changing variables  $\tilde{s} = s/\epsilon$ ,  $\tilde{r} = r/\epsilon$  and using the fact that

$$\int_{-\infty}^{\infty} \operatorname{sech}(x - y)\operatorname{sech}(y) dy = 2x \operatorname{csch}(x), \quad (45)$$

the contribution from the double integral in the first region can be readily obtained. Contributions from the other two regions can be calculated in a similar manner, and they turn out to be the same as that from the first region.

With the change of variables  $U(x, y, \xi) = e^{-i\kappa_0 w} \widehat{U}(x, y, \xi)$ , we then find that near the singularity the full integral equation (21) reduces to the inner equation

$$\begin{aligned} L_0 \widehat{U} + \epsilon\xi L_1 \widehat{U} + \epsilon^2(\eta - \xi^2) \widehat{U} + \frac{3}{2\epsilon^2} \sigma \alpha^2 \beta^2 b(x, y)^3 \\ \times \int_{-\infty}^{\infty} \omega e^{\pi\beta\omega/2} \operatorname{csch}\left(\frac{\pi\beta\omega}{2}\right) \Phi_0(\xi - \omega) d\omega = 0. \end{aligned} \quad (46)$$

After substituting in the expansion (41), at  $O(\epsilon^{-4})$  and  $O(\epsilon^{-3})$  the above equation is automatically satisfied; and at  $O(\epsilon^{-2})$  the equation governing  $\Phi_0(\xi)$  is found from the solvability condition as

$$(1 + \beta^2 \xi^2) \Phi_0 - 3\beta^2 \int_{-\infty}^{\infty} \omega e^{\pi\beta\omega/2} \operatorname{csch}\left(\frac{\pi\beta\omega}{2}\right) \Phi_0(\xi - \omega) d\omega = 0. \quad (47)$$

This is a linear homogeneous Fredholm integral equation which has been solved before [8, 16]. Its analytic solution in the region  $|\operatorname{Imag}(\xi)| \geq 1/\beta$  is

$$\Phi_0(\xi) = \frac{6\beta^4}{1 + \beta^2 \xi^2} \int_0^{\pm i\infty} \frac{1}{\sin^2 s} \phi(s) e^{-s\beta\xi} ds, \quad (48)$$

where the plus sign in the contour is for  $\text{Imag}(\xi) \leq -1/\beta$ , the minus sign for  $\text{Imag}(\xi) \geq 1/\beta$ ,

$$\phi(s) = C \left( \frac{2}{\sin s} + \frac{\cos^2 s}{\sin s} - \frac{3s \cos s}{\sin^2 s} \right), \quad (49)$$

and  $C$  is a complex constant. Clearly this solution has simple-pole singularities at  $\xi = \pm i/\beta$ . Since the integral of (48) at these points is equal to  $-C/6$ , we see that

$$\Phi_0(\xi) \sim -\frac{C\beta^4}{1 + \beta^2\xi^2}, \quad \text{for } \xi \rightarrow \pm \frac{i}{\beta}, \quad (50)$$

thus the pole has strength  $\pm i\beta^3 C/2$  at  $\xi = \pm i/\beta$ . After substituting this back into equation (41) and changing variables to  $K = \kappa_0/\epsilon + \xi$ , we find that  $U(x, y, K)$  has simple poles at  $K = \kappa_0/\epsilon \pm i/\beta$ , and

$$U(x, y, K) \sim \pm \frac{i\beta^3 C}{2\epsilon^4} e^{-i\kappa_0 w} b(x, y) \frac{1}{K - \left(\frac{\kappa_0}{\epsilon} \pm \frac{i}{\beta}\right)} \quad \text{for } K \rightarrow \frac{\kappa_0}{\epsilon} \pm \frac{i}{\beta}. \quad (51)$$

Finally, from Eq. (18), we obtain the local behavior of  $\hat{\psi}(x, y, K)$  near the simple poles  $K = \kappa_0/\epsilon \pm i/\beta$  as

$$\hat{\psi}(x, y, K) \sim \frac{\beta^3 C}{\epsilon^3} e^{-\pi\beta\kappa_0/2\epsilon} e^{\pm W_0/\beta} \frac{e^{-i\kappa_0(w+w_0)}}{K - \left(\frac{\kappa_0}{\epsilon} \pm \frac{i}{\beta}\right)} b(x, y), \quad K \rightarrow \frac{\kappa_0}{\epsilon} \pm \frac{i}{\beta}, \quad (52)$$

where

$$w_0 = W_0/\epsilon.$$

Moreover, from the symmetry of the Fourier transform

$$\hat{\psi}(x, y, K) = \hat{\psi}^*(x, y, -K^*) \quad (53)$$

for real functions  $\psi(x, y, W)$ , we also deduce the local behavior of  $\hat{\psi}(x, y, K)$  near the simple poles  $K = -\kappa_0/\epsilon \pm i/\beta$ .

From the above local analysis, the residues of these poles are only determined up to a constant multiple ( $C$  is unknown at the moment). To determine  $C$ , we match the large- $\xi$  asymptotics of the above inner solution for  $U$  with the outer solution for  $U$  away from the singularities, in the matching region  $1 \ll |\xi| \ll \epsilon^{-1}$ . To this end, we note that for  $|\xi| \gg 1$  the main contribution of the integral in solution (48) comes from the region  $s \approx 0$  where  $\phi(s) \sim \frac{2}{5}Cs^3$ . This yields

$$\Phi_0(\xi) \sim \frac{12C}{5} \frac{1}{\xi^4}, \quad \text{for } |\xi| \gg 1. \quad (54)$$

Putting this back into equation (41), we find the following large- $\xi$  behavior for the inner solution,

$$U(x, y, \kappa) \sim \frac{12C}{5} \frac{b(x, y)}{(\kappa - \kappa_0)^4} e^{-i\kappa_0 w}. \quad (55)$$

As discussed in section 5, this behavior matches to the outer solution with  $|\kappa - \kappa_0| \ll 1$ .

## 7 Inversion of Fourier transform and true line solitons

We now take the inverse Fourier transform of (16),

$$\psi(x, y, W) = \int_{\mathcal{C}} \widehat{\psi}(x, y, K) e^{iKW} dK \quad (56)$$

in order to determine the tail behaviors in the physical solution  $\psi(x, y, W)$ . Here  $\widehat{\psi}(x, y, K)$  is given by Eq. (18). As explained in [8], if we require this physical solution to decay upstream ( $w \rightarrow -\infty$ ), then the contour  $\mathcal{C}$  in this inverse Fourier transform should be taken along the line  $\text{Imag}(K) = -1/\beta$  and pass below the poles  $K = \pm\kappa_0/\epsilon - i/\beta$ . It should also pass above the pole  $K = -i/\beta$  of the  $\text{sech}(\pi\beta K/2)$  term in Eq. (18). Then when  $w \gg 1$  (downstream), by completing the contour  $\mathcal{C}$  with a large semicircle in the upper half plane, we pick up dominant contributions from the pole singularities at  $K = \pm\kappa_0/\epsilon - i/\beta$  and  $K = i/\beta$ . Collecting these pole contributions, the wave profile of the solution far downstream is then found to be

$$\begin{aligned} \psi \sim & 2\epsilon\alpha e^{-(W-W_0)/\beta} b(x, y) \\ & + \frac{4\pi\beta^3 C_0}{\epsilon^3} e^{-\pi\beta\kappa_0/2\epsilon} \sin(\kappa_0 w_0 - \Theta_0) e^{(W-W_0)/\beta} b(x, y), \quad w \gg 1/\epsilon, \end{aligned} \quad (57)$$

where  $C_0 > 0$  and  $\Theta_0$  are the amplitude and phase of the constant  $C$  (which is complex in general), i.e.,  $C = C_0 e^{i\Theta_0}$ .

For this solution to be a line soliton, the growing term in (57) must vanish so  $\sin(\kappa_0 w_0 - \Theta_0) = 0$ . Thus, there are two allowable locations for line solitons (relative to the lattice),

$$w_0 = \Theta_0/\kappa_0, \quad (\pi + \Theta_0)/\kappa_0. \quad (58)$$

Line solitons at these two locations are called onsite and offsite solitons respectively. For the particular lattice (15) and  $\sigma = 1$ , these two line solitons near the edge of the semi-infinite gap with  $\tan\theta = 1, 2$  are displayed in Fig. 1. For these solitons,  $\Theta_0 = 0$  since  $C$  is real positive (see equations (38) and (39)).

The above results show that for any rational slope  $\tan\theta$ , two line solitons with envelope locations (58) exist in a general two-dimensional lattice. What if the slope is irrational? Treating an irrational number as the limit of a rational number  $p/q$  with  $p, q \rightarrow \infty$ , then  $\kappa_0 = \sqrt{p^2 + q^2} \rightarrow \infty$ , hence the growing tail downstream in (57) vanishes. This suggests that for an irrational slope, line solitons exist for arbitrary envelope positions  $w_0$ . But we cannot numerically verify this conjecture since irrational numbers cannot be represented accurately on computers.

Finally, if one wishes to obtain line wave packets  $\psi(x, y, W)$  which decay for  $w \rightarrow +\infty$  but contain a growing tail for  $w \ll -1$ , then the contour  $\mathcal{C}$  in the inverse Fourier transform should be taken along the line  $\text{Imag}(K) = 1/\beta$  and pass above the poles  $K = \pm\kappa_0/\epsilon + i/\beta$  and below the pole  $K = i/\beta$ . Then when  $w \ll -1$ , by completing the contour  $\mathcal{C}$  with a large semicircle in the lower half plane and picking up dominant pole contributions, the wave profile of the solution is found to be

$$\begin{aligned} \psi \sim & 2\epsilon\alpha e^{(W-W_0)/\beta} b(x, y) \\ & - \frac{4\pi\beta^3 C_0}{\epsilon^3} e^{-\pi\beta\kappa_0/2\epsilon} \sin(\kappa_0 w_0 - \Theta_0) e^{-(W-W_0)/\beta} b(x, y), \quad w \ll -1/\epsilon. \end{aligned} \quad (59)$$

This ‘flipped’ wave solution will be useful when we construct multi-line-soliton bound states in the next section.

## 8 Construction of multi-line-soliton bound states

The asymptotic tail formula (57) can be used not only to determine the locations of line solitons, but also to construct multi-line-soliton bound states. These bound states are analytically constructed by matching the downstream growing tail of a line wavepacket with the upstream decaying tail of another line wavepacket. This technique has been used for the construction of one-dimensional multi-soliton bound states before [9, 10, 16]. Here we apply the same principle to the construction of multi-line soliton solutions in a general two-dimensional lattice potential.

Consider the asymptotic expansion of two line wavepackets centered at  $w_1 = W_1/\epsilon$  (left) and  $w_2 = W_2/\epsilon$  (right) receptively. The left wavepacket decays for  $w - w_1 \ll -1$  and has a growing exponential tail for  $w - w_1 \gg 1$ , and the right wavepacket decays for  $w - w_2 \gg 1$  and has a growing exponential tail for  $w - w_2 \ll -1$ . For line-soliton bound states, the decaying and growing tails of the two wavepackets must match in the region  $w_1 \ll w \ll w_2$ . In this matching region, the left wavepacket's asymptotics is given by (57) with  $w_0$  replaced by  $w_1$ , and the right wavepacket's asymptotics is given by (59) with  $w_0$  replaced by  $w_2$ . Matching of these asymptotics results in the following system of equations

$$\begin{aligned} 2\epsilon\alpha e^{-(W-W_1)/\beta} b(x, y) &= \mp \frac{4\pi\beta^3 C_0}{\epsilon^3} e^{-\pi\beta\kappa_0/2\epsilon} \sin(\kappa_0 w_2 - \Theta_0) e^{-(W-W_2)/\beta} b(x, y), \\ 2\epsilon\alpha e^{(W-W_2)/\beta} b(x, y) &= \pm \frac{4\pi\beta^3 C_0}{\epsilon^3} e^{-\pi\beta\kappa_0/2\epsilon} \sin(\kappa_0 w_1 - \Theta_0) e^{(W-W_1)/\beta} b(x, y), \end{aligned}$$

where the  $\mp$  comes from the possible  $\pi$  phase shift between the two wavepackets. After simplification, these matching conditions read

$$\sin(\kappa_0 w_1 - \Theta_0) = -\sin(\kappa_0 w_2 - \Theta_0) = \pm \frac{\alpha\epsilon^4}{2\pi\beta^3 C_0} e^{\pi\beta\kappa_0/2\epsilon} e^{\epsilon(w_1 - w_2)/\beta}. \quad (60)$$

With a change of variables  $\hat{w}_1 = -(w_1 - \Theta_0/\kappa_0)$ ,  $\hat{w}_2 = w_2 - \Theta_0/\kappa_0$ , the above matching conditions then become almost identical to the ones derived in [9] before. As has been explained there, this system of equations admits an infinite number of solutions for each fixed  $\epsilon > 0$ . Varying  $\epsilon$ , then infinite families of two-line soliton bound states are obtained.

Note that for equations (60) to have a solution, the right-hand side must have magnitude less than one. Since this is not the case as  $\epsilon \rightarrow 0$  for any finite distance  $w_2 - w_1$  between the two line wavepackets, bifurcations of these bound states occur at finite amplitude away from the band edge. In figure 4, we show a particular family of bound states in the lattice (15) with  $\sigma = 1$  and  $\tan\theta = 1$ . This family bifurcates at  $\mu \approx 4.073$  (near the edge  $\mu_0 = 4.1264$  of the semi-infinite gap). As predicted by the analysis of equation (60) in [9], this solution family contains three connected branches, and their power curve is shown in Fig. 4 (upper left panel). Here the power is calculated over one period along the line-soliton direction  $w' = x \cos\theta + y \sin\theta$ , which is  $\pi\sqrt{p^2 + q^2}$  in the present case. Profiles of bound states at  $\mu = 4.0639$  of the three power branches are displayed in Fig. 4 (A,B,C). The bound state in the A panel comprises roughly two onsite line solitons, the one in the B panel comprises roughly an onsite and an offsite line solitons, and the bound state in the C panel comprises roughly two offsite line solitons.

We would like to point out that the above construction of infinite families of line-soliton bound states was performed for general two-dimensional lattices. This contrasts the earlier work in [9, 10] where such construction was made only for symmetric one-dimensional lattices (where  $\Theta_0 = 0$ ). From the above calculations, it is now clear that the previous derivation of multi-soliton bound states in [9, 10] can be extended to general one-dimensional lattices, too.

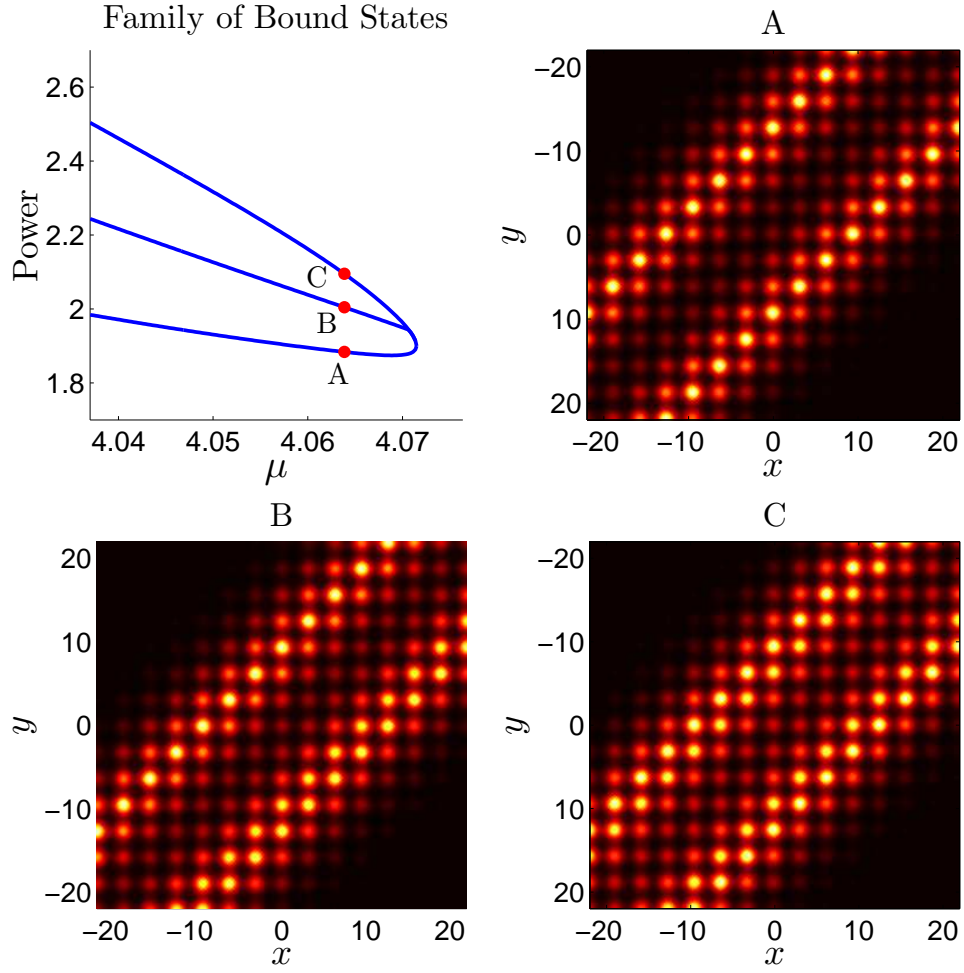


Figure 4: (Color online) Power curve and solution profiles in a family of two-line soliton bound states in the lattice (15) with  $\sigma = 1$  and  $\tan \theta = 1$ .

## 9 Connection to zero-eigenvalue bifurcations

In this section, we consider the linear stability eigenvalues of single-line solitons as obtained in section 7. Our interest lies in the pair of exponentially small eigenvalues of these solitons, which bifurcate out from the origin at the band edge; the associated eigenfunctions have zero wavenumber along the line-soliton direction (i.e., are periodic along the line direction with the period matching that of the line soliton). Such eigenvalues can be analytically calculated from the tail asymptotics (57) of line wavepackets which we have derived. Thus, by comparing the analytical formula of these eigenvalues with the numerically computed eigenvalues, we can quantitatively verify the formula in Eq. (57) for the exponentially small growing tails. We do caution, however, that we are ignoring other eigenvalues whose eigenfunctions have nonzero wavenumber along the line-soliton direction, and those eigenvalues are often more unstable [14, 15]. Thus the eigenvalue calculation in this section does not constitute a full stability analysis.

The present calculation of zero-eigenvalue bifurcation closely parallels that in one-dimensional problems [19, 8, 10]. Let  $\psi_s(x, y) = \psi(x, y; w_{0s})$  be a single-line soliton solution of equation (3) with center at  $w_0 = w_{0s}$ , which decays to zero as  $w \rightarrow \pm\infty$  and is periodic along the line direction,  $w' = x \cos \theta + y \sin \theta$ , with period matching that of the Bloch wave. Perturbing this line soliton by normal modes

$$\Psi = e^{-i\mu t} \left[ \psi_s + (v + \varphi)e^{\lambda t} + (v^* - \varphi^*)e^{\lambda^* t} \right], \quad (61)$$

with  $v, \varphi \ll 1$ , we obtain the linear-stability eigenvalue problem

$$\mathcal{L}_0 \mathcal{L}_1 v = -\lambda^2 v, \quad (62)$$

where

$$\mathcal{L}_0 = \nabla^2 + \mu - V(x, y) + \sigma \psi_s^2, \quad \mathcal{L}_1 = \nabla^2 + \mu - V(x, y) + 3\sigma \psi_s^2,$$

and  $\lambda$  is the stability eigenvalue. Since the bifurcated eigenvalue  $\lambda$  is small near band edges, we expand the eigenfunction  $v$  into a perturbation series

$$v = v_0 + \lambda^2 v_1 + \lambda^4 v_2 + \dots \quad (63)$$

Inserting this expansion into Eq. (62), at  $O(1)$  we get

$$L_0 L_1 v_0 = 0. \quad (64)$$

A solution to this equation is

$$v_0 = (\partial\psi/\partial w_0)_{w_0=w_{0s}}. \quad (65)$$

Recalling the perturbation series expansion of  $\psi(x, y; w_0)$  in Eq. (7) as well as the envelope solution in Eq. (13), we find that

$$v_0 \sim -\frac{\epsilon^2 \alpha}{\beta} \operatorname{sech} \frac{\epsilon(w - w_{0s})}{\beta} \tanh \frac{\epsilon(w - w_{0s})}{\beta} b(x, y).$$

From this equation it is seen that the eigenfunction  $v$  is periodic along the line-soliton direction  $w' = x \cos \theta + y \sin \theta$ , with period matching that of the Bloch wave (and the line soliton), so the net wavenumber of this eigenfunction along the line-soliton direction is zero.

From the large- $w$  asymptotics (57) of the solution  $\psi(x, y; w_0)$ , we see that when  $w \gg 1/\epsilon$ ,  $v_0$  contains a growing tail,

$$v_0 \sim \pm \epsilon^{-3} 4\pi\beta^3 \kappa_0 C_0 e^{-\pi\beta\kappa_0/2\epsilon} e^{\epsilon(w-w_{0s})/\beta} b(x, y). \quad (66)$$

Here the plus and minus sign correspond to the onsite and offsite line solitons, respectively. This growing tail must be balanced by the higher-order terms in the expansion (63), thereby yielding an analytical formula for the eigenvalue  $\lambda$ . Carrying out this program as in [8, 10, 19], we find that

$$\lambda^2 = \mp C_0 \frac{32\pi\kappa_0\beta^4}{\alpha\epsilon} e^{-\pi\beta\kappa_0/2\epsilon}. \quad (67)$$

Thus this eigenvalue is stable for onsite line solitons and unstable for offsite ones, and its magnitude is exponentially small.

A comparison of the analytical prediction (67) for the eigenvalue to numerical results for offsite line solitons is presented in Fig. 5 for the lattice (15) with  $\sigma = 1$  and  $\tan\theta = 1, 2$ . It is seen that the analytical and numerical eigenvalues agree with each other very well. Notice that the analytical eigenvalue formula contains the constant  $C_0$ , and the ratio of  $\lambda^2/[32\pi\kappa_0\beta^4 e^{-\pi\beta\kappa_0/2\epsilon}/\alpha\epsilon]$  approaches  $C_0$  when  $\epsilon \rightarrow 0$ . We have plotted this ratio for numerically obtained eigenvalues in the right panels of Fig. 5. It is seen that as  $\epsilon \rightarrow 0$ , this ratio indeed approaches the  $C$  value obtained from equations (38) and (39) in section 5. Thus our formula (57) for the exponentially-small growing tails in line wavepackets is fully verified quantitatively.

## 10 Further examples with asymmetric potentials

To help demonstrate the generality of our theory, we now consider the asymmetric lattice

$$V(x, y) = \frac{3}{2}(\sin 2x + \sin 4x + \sin 2y + \sin 4y), \quad (68)$$

which is shown in Fig. 6 (top left panel). For this lattice, the edge of the semi-infinite gap is  $\mu_0 = -0.6891$ . With soliton inclination  $\tan\theta = -1$  and nonlinearity coefficient  $\sigma = 1$ , we find the two soliton families which bifurcate off this band edge (see Fig. 6, bottom panel). In this case numerical solution of the ‘‘outer’’ integral equation (30) yields a complex value for  $C = C_0 e^{i\Theta_0}$ ,

$$C_0 = 8.25, \quad \Theta_0 = 2.66, \quad (69)$$

see Fig. 6 (top right panel). This  $\Theta_0$  value in turn gives the center of the solitons, from formulae (58), as  $w_0 = 0.94$  and  $2.05$  for onsite and offsite, respectively (up to periodic repetitions in the lattice). Comparison of this prediction with the envelope locations of numerically obtained solitons shows good agreement (see Fig. 6, bottom panel).

## 11 Line solitons bifurcated from interior points of Bloch bands

In previous sections, we studied line solitons that bifurcate from edges of Bloch bands. But line solitons can also bifurcate from high-symmetry points inside Bloch bands, as has been reported numerically and experimentally before [13, 14, 15]. Here the high-symmetry points are points on the dispersion surface  $\mu = \mu(k_x, k_y)$  where  $\partial\mu/\partial k_x = \partial\mu/\partial k_y = 0$ , with  $k_x, k_y$  being the Bloch

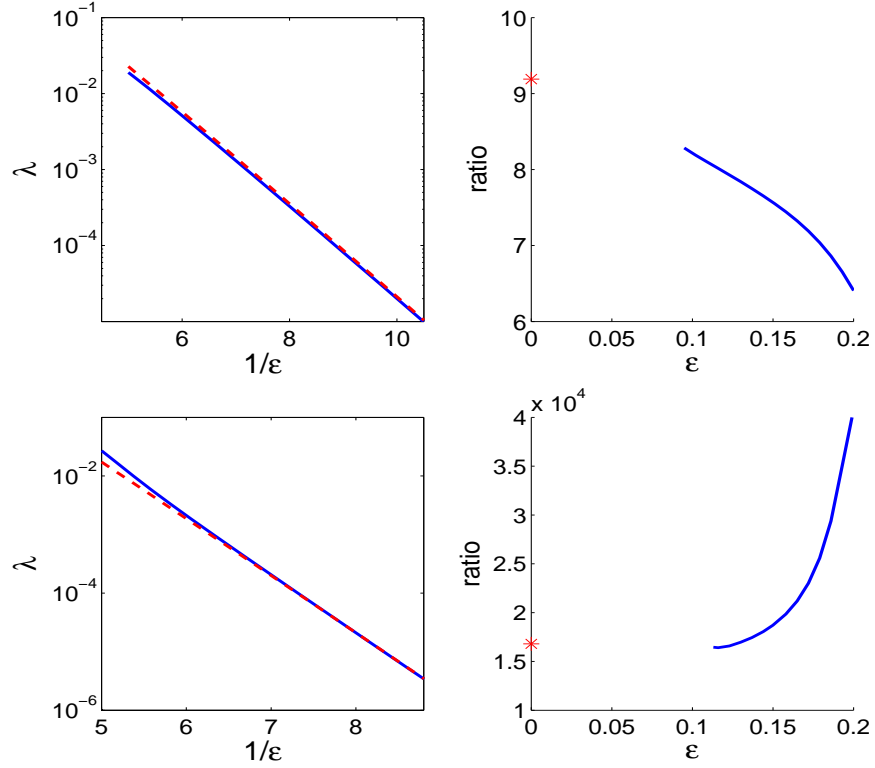


Figure 5: Eigenvalue comparison for offsite line solitons with  $\sigma = 1$  and lattice (15): (top)  $\tan \theta = 1$ ; (bottom)  $\tan \theta = 2$ . (Left) Numerically calculated  $\lambda$  value in solid blue and the asymptotic approximation in dashed red. (right) The value for  $C$  left from taking the ratio of the numerical eigenvalues and the asymptotic expression as well as the predicted limiting value (red star) from equations (38) and (39) in section 5.

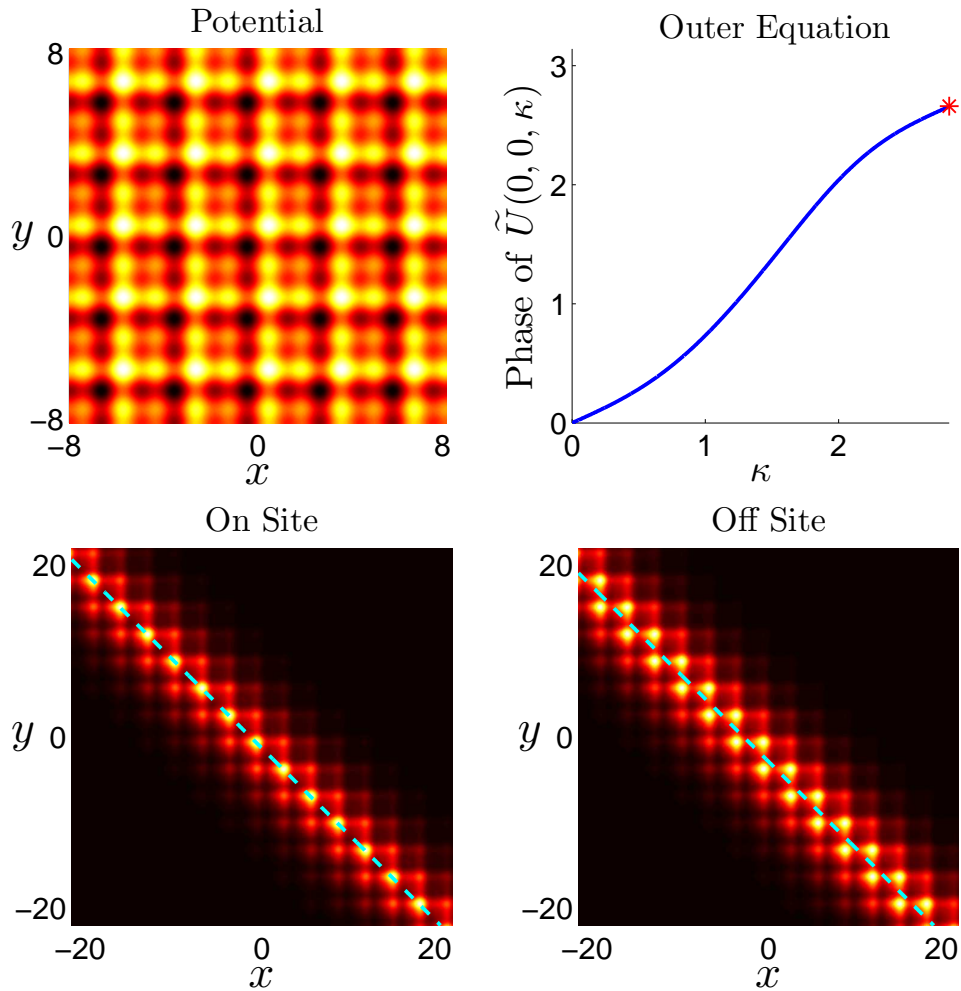


Figure 6: (Color online) Line solitons in the asymmetric lattice (68) with  $\sigma = 1$  and  $\tan \theta = -1$ . (Top left) the potential (68). (Top right) the phase calculated from the “outer” integral equation (30); the asterisk marks the phase value  $\Theta_0$  at the singularity  $\kappa_0 = 2\sqrt{2}$ . (Bottom) onsite and offsite line solitons for  $\epsilon = 0.35$  as well as the predicted centers of the solitons (dashed).

wavenumbers in the  $x$  and  $y$  directions. For line solitons bifurcated from such interior points of Bloch bands, however, resonance with Bloch modes may occur. Such resonance excites Bloch-wave tails that are non-vanishing in the direction perpendicular to the line and hence makes the line “soliton” nonlocal [20]. To obtain true line solitons inside Bloch bands, this resonance must be absent, a requirement that poses strong restrictions on the angles of line solitons. Indeed, we will see below that inside Bloch bands, line solitons at only a couple of special angles are admissible.

First we consider a concrete example with the lattice

$$V(x, y) = 6 \sin^2 x + 4 \sin^2 y. \quad (70)$$

Inside the first Bloch band,  $\mu \in [3.6080, 4.1565]$ , of this lattice there is an X-symmetry point

$$(k_{x0}, k_{y0}, \mu_0) = (0, 1, 3.9529), \quad (71)$$

whose Bloch mode is  $\pi$ -periodic in  $x$  and  $2\pi$ -periodic in  $y$ . The dispersion surface near this X-point is saddle-shaped. For line solitons bifurcating from this X-point,  $\mu = \mu_0 + \eta\epsilon^2$ ,  $\eta = \pm 1$ , and  $\epsilon \ll 1$ . Taking  $\epsilon = 0.2$ , the level curves of the dispersion surface at  $\mu(k_x, k_y) = \mu_0 + \eta\epsilon^2$  for  $\eta = \pm 1$  are displayed in Fig. 7 (left panels, solid lines).

Suppose the angle of the line soliton with the  $x$ -axis is  $\theta$ . Then at the  $\mu$  value of the line soliton, linear Bloch modes that are periodic along this line direction, with the period matching that of the X-point Bloch wave, are located in the wavenumber plane at the intersections of the parametrically defined line

$$k_x = \kappa_0 \sin \theta + k_{x0}, \quad (72a)$$

$$k_y = -\kappa_0 \cos \theta + k_{y0}, \quad (72b)$$

with the level curve

$$\mu(k_x, k_y) = \mu_0 + \eta\epsilon^2. \quad (73)$$

Existence of such intersections means that the line soliton is in resonance with Bloch modes.

Inspection of the level curves in Fig. 7 shows that for almost all angles  $\theta$ , the line (72), whose slope is  $-\cot \theta$ , always intersects those level curves for both  $\eta = \pm 1$ . The only exceptions are  $\theta = 0, \pm\pi/4$  for  $\eta = 1$  and  $\theta = \pi/2$  for  $\eta = -1$ . In these cases, resonance is absent, thus true line solitons could exist. Recalling the conditions for envelope solitons below Eq. (12), we see that true line solitons with angles  $\theta = 0, \pm\pi/4$  may bifurcate from the X-point (71) under defocusing nonlinearity ( $\sigma = -1$ ), and true line solitons with angle  $\theta = \pi/2$  may bifurcate from this X-point under focusing nonlinearity ( $\sigma = 1$ ). But where are the envelope positions of these bifurcating line solitons inside Bloch bands? To answer this question, it is again necessary to use exponential asymptotics.

Strictly speaking, our exponential-asymptotics analysis in the previous sections was for line solitons bifurcating from edges of Bloch bands and residing outside of them (thus resonance with Bloch bands never occurs). But for line solitons with special angles inside Bloch bands, those which avoid resonance, our previous analysis can be applied without any additional work. The conclusion is that, for each of those special angles, two families of line solitons, one onsite and the other offsite, bifurcate out from this X-symmetry point; and their envelope locations are given by the formulae (58). Numerically we have confirmed these predictions. For instance, the onsite line solitons near the X-point (71), at angle  $\theta = \pi/4$  for defocusing nonlinearity and at angle  $\theta = \pi/2$

for focusing nonlinearity, have been numerically obtained and displayed in Fig. 7 (right panels); and their envelope locations agree with those predicted by the formulae (58). Our analytical results are consistent with the numerical and experimental reports of line solitons inside Bloch bands in [13, 14, 15] as well.

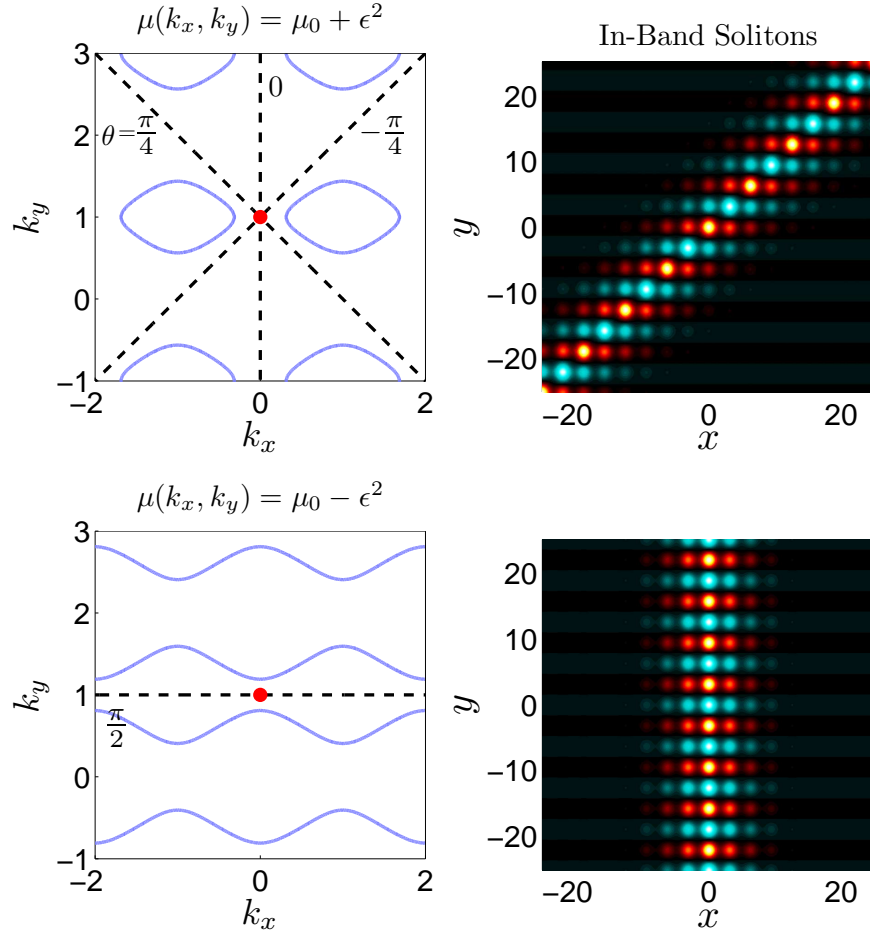


Figure 7: (Color online) In-band line solitons in the lattice (70) near the X-symmetry point  $(k_x, k_y) = (0, 1)$  at special angles for  $\epsilon = 0.2$ . Top:  $\eta = 1$  and  $\sigma = -1$  (defocusing nonlinearity). Bottom:  $\eta = -1$  and  $\sigma = 1$  (focusing nonlinearity). Left: level curves  $\mu(k_x, k_y) = \mu_0 + \eta\epsilon^2$  extended periodically (solid) and the line (72) (dashed) for values of angle  $\theta$  which admit true line solitons. Right: onsite line solitons at these special angles with  $\mu = \mu_0 + \eta\epsilon^2$ .

As explained above, inside Bloch bands, line solitons for most inclination angles are nonlocal (in the normal direction), in the sense that they comprise non-vanishing Bloch-wave tails far away from the central line. Then a natural question is, how can we determine the amplitudes of those non-vanishing Bloch-wave tails? It turns out that this question can also be treated in the framework of the exponential-asymptotics theory developed above. Specifically, we should first recognize that the  $\kappa_0$  value at the intersection of the line (72) and the level curve (73) also satisfies equation (22) for singularity locations (which can be easily checked). Thus this  $\kappa_0$  value of resonant Bloch

modes is also a real pole in the Fourier transform  $\widehat{\psi}(x, y, K)$  of the nonlocal line-soliton solution  $\psi(x, y, W)$ . Unlike the fourth-order poles (26) in our earlier analysis (see Eq. (35)), this resonant pole is simple (i.e., first-order). The residue of this resonant pole is also exponentially small in  $\epsilon$ , and its exact value can be computed from the same outer integral equation (30) by the same numerical algorithm (32) in the earlier text. From the residue of this resonant pole and the inverse Fourier transform (56), the amplitudes of non-vanishing Bloch-wave tails in the nonlocal line solitons will then be obtained. This problem of calculating amplitudes of non-vanishing Bloch-wave tails in nonlocal line solitons resembles that of calculating amplitudes of continuous-wave tails in the fifth-order Kortewegde Vries equation, the third-order NLS equation and other related equations [5, 21, 22, 23, 24, 25, 26]. But our treatment of directly solving the outer integral equation for the residues of resonant poles differs from those earlier one-dimensional works, which hinge on the recurrence relation for the coefficients of the Taylor expansion of the Fourier transform.

The results from the above specific example hold qualitatively for all line solitons inside Bloch bands. Specifically, inside Bloch bands true line solitons exist only for very few (up to three) special angles due to the requirement of resonance suppression. For each of those special angles, there exist two line solitons, one onsite and the other offsite.

## 12 Conclusion

In this paper, we have presented what we believe is the first step toward a fully two-dimensional asymptotic theory for the bifurcation of solitons from infinitesimal continuous waves. For line solitons bifurcating from infinitesimal Bloch waves in a general two-dimensional periodic potential, an analytical theory utilizing exponential asymptotics is developed. For this two-dimensional problem, the previous approach of relying on a certain recurrence relation to solve the outer integral equation is no longer viable due to the presence of complex poles which are closer to the origin than the real poles. Instead, we solved this outer equation directly along the real line up to the real poles. This new approach not only overcomes the recurrence-relation limitation, but also simplifies the exponential-asymptotics process.

Using this modified technique, we showed that from every edge of the Bloch bands, line solitons with any rational line slope bifurcate out; and for each rational slope, two line-soliton families exist. In addition, a countable set of multi-line-soliton bound states have been constructed analytically. Furthermore, as a byproduct of this exponential-asymptotics theory, a certain linear-stability eigenvalue that bifurcates out of the origin at a band edge, is analytically obtained. Line solitons bifurcating from interior points of the Bloch bands were investigated as well, and it was shown that such solitons exist (inside Bloch bands) only for a couple of very special line angles due to resonance with the Bloch bands. These analytical predictions were compared with numerical results for symmetric as well as asymmetric potentials, and good qualitative and quantitative agreement was obtained.

Throughout the analysis, the potential in Eq. (1) is taken to be in minimal-period orientation. If the potential is not aligned along that minimal-period orientation, all our results would still hold, except that the smallest of the real poles in Eq. (26) would not be those given by Eq. (28), but rather be a certain multiple of those numbers.

In this article, we assumed that the potential in Eq. (1) has equal periods in  $x$  and  $y$ . If the  $x$ - and  $y$ -periods are not the same, say  $\pi$  in  $x$  and  $\chi\pi$  in  $y$ , with  $\chi$  being the ratio between the two periods, then we can introduce the scaled  $y$  variable  $\hat{y} = y/\chi$ . In this scaled variable, the periods

of the potential are  $\pi$  in both  $x$  and  $\hat{y}$ , hence satisfying the assumption in this paper. Due to this  $y$ -scaling, the Laplacian  $\nabla^2$  in Eq. (1) changes to  $\partial_{xx} + \chi^{-2}\partial_{\hat{y}\hat{y}}$ . For this scaled ‘‘Laplacian’’, all our analysis is still valid (except for very minor modifications), because our analysis does not rely on the equal coefficients in the Laplacian at all. Following this analysis, we shall find that from every edge of the Bloch bands, line solitons with slopes of any rational number divided by  $\chi$  bifurcate out; and for each of those slopes, two line-soliton families exist. We shall also find that from a high-symmetry point inside Bloch bands, line solitons at only a couple of special angles may bifurcate out.

Finally, we point out that the analysis in this paper is developed for line solitons bifurcating from high-symmetry points of the Bloch bands where the Bloch mode is unique (see Assumption 1). At certain points of the Bloch bands, however, the Bloch modes are not unique [27]. In such cases, nonlinear interactions between different Bloch modes would occur [27]. To treat line-soliton bifurcations from such Bloch-band points, the exponential asymptotics analysis of this article would need to be generalized. Such generalizations will be left for future studies.

## Acknowledgment

This work is supported in part by the Air Force Office of Scientific Research under grant USAF 9550-12-1-0244.

## Appendix: Line solitons in stripe lattices

In this appendix, we consider line solitons in stripe lattices, i.e., lattices which vary only in one direction  $V(x, y) = V(x)$ . We shall show that line solitons in such lattices only have complex poles and no real poles. In addition, the envelopes of these solitons can be arbitrarily located. Our conclusion will be that complex poles do not place restrictions on envelope locations.

The bulk of the analysis remains the same as in the main text. We consider stationary solutions whose leading-order term is a Bloch-wave packet,

$$\psi(x, y, W) \sim \epsilon A(W - W_0)b(x). \quad (74)$$

The packet envelope  $A(W - W_0)$  has a sech-profile and varies only in the direction of  $W = \epsilon(x \sin \theta - y \cos \theta)$ , and  $W_0 = \epsilon x_0$  is the location of this envelope.

The pole singularities of these line wavepackets are the values of  $\kappa_0$  where Eq. (22) holds, except that the operator  $L_0$  drops the  $y$ -dependence now. That is,

$$L_0\phi + i\kappa_0 L_1\phi - \kappa_0^2\phi = 0, \quad (75)$$

and

$$L_0 = \partial_x^2 + \mu_0 - V(x), \quad L_1 = 2\nabla \cdot [\sin \theta, -\cos \theta]. \quad (76)$$

Converting this equation into the eigenvalue problem (27), we find that all eigenvalues  $\kappa_0$  are now complex-valued and not real (excluding 0). This is illustrated in figure 8 (right panel). Here the lattice is chosen as  $V(x) = 6 \sin^2 x$  and the line slope as  $\tan(\theta) = 1$ .

In this stripe lattice, we have numerically found line solitons. An example with  $\sigma = 1$  is shown in figure 8 (left panel). Since the lattice is  $y$ -independent, so are the Bloch modes  $b(x)$ . Then if

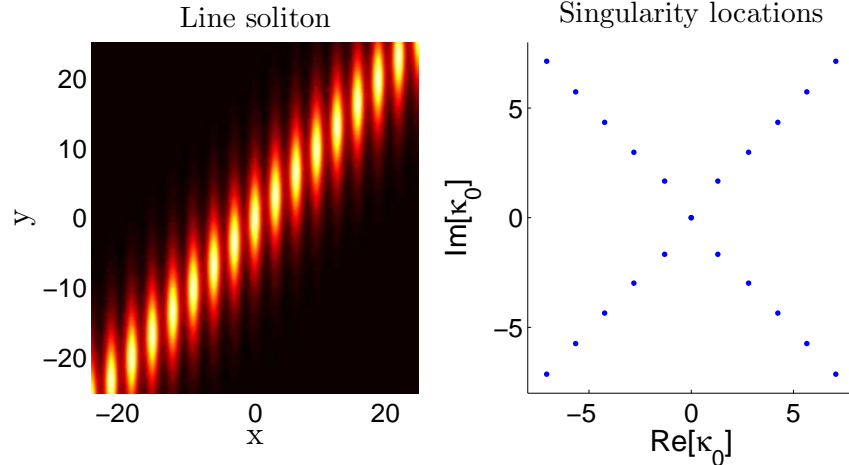


Figure 8: (Color online) A line soliton (left) and its singularity structure (right) for the stripe lattice  $V(x) = 6 \sin^2 x$  with  $\tan \theta = 1$  and  $\sigma = 1$ .

a line soliton exists with the envelope centered at a particular  $W_0$  value, from equation (74) it is clear that line solitons with the envelope centered at arbitrary  $W_0$  values would exist, because any variation in  $W_0$  may be compensated for by a shift in the  $y$  coordinate of  $W$ .

From the above analysis, we conclude that in a stripe lattice, envelopes of line solitons can be arbitrarily positioned, and poles of those solitons are all complex-valued (off the real axis).

## References

- [1] Y. S. Kivshar and G. P. Agrawal. *Optical Solitons: From Fibers to Photonic Crystals* (Academic Press, San Diego, 2003).
- [2] M. Skorobogatiy and J. Yang, *Fundamentals of Photonic Crystal Guiding* (Cambridge University Press, Cambridge, UK, 2009).
- [3] O. Morsch and M. Oberthaler, “Dynamics of Bose-Einstein condensates in optical lattices”, *Rev. Mod. Phys.* 78, 179–215 (2006).
- [4] P.G. Kevrekidis, D.J. Frantzeskakis and R. Carretero-Gonzalez, editors, *Emergent Nonlinear Phenomena in Bose-Einstein Condensates* (Springer, Berlin, 2008).
- [5] J. Yang, *Nonlinear Waves in Integrable and Nonintegrable Systems* (SIAM, Philadelphia, 2010).
- [6] T. Dohnal, D. Pelinovsky, and G. Schneider, “Coupled-mode equations and gap solitons in a two-dimensional nonlinear elliptic problem with a separable potential”, *J. Nonlinear Sci.*, 19, 95-131 (2009).
- [7] B. Ilan and M.I. Weinstein, “Band-edge solitons, nonlinear Schrödinger/GrossPitaevskii equations, and effective media”, *Multiscale Model. Simul.* 8, 1055–1101 (2010).

- [8] G. Hwang, T. R. Akylas, and J. Yang, “Gap solitons and their linear stability in one-dimensional periodic media”, *Physica D* 240, 1055–1068 (2011).
- [9] T. R. Akylas, G. Hwang, and J. Yang, “From non-local gap solitary waves to bound states in periodic media”, *Proc. R. Soc. A* 468, 116–135 (2012).
- [10] G. Hwang, T. R. Akylas, and J. Yang, “Solitary waves and their linear stability in nonlinear lattices”, *Stud. Appl. Math.* 128, 275–299 (2012).
- [11] Z. Chen, H. Martin, E. D. Eugenieva, J. Xu, and A. Bezryadina, “Anisotropic enhancement of discrete diffraction and formation of two-dimensional discrete-soliton trains”, *Phys. Rev. Lett.* 92, 143902 (2004).
- [12] C. Lou, X. Wang, J. Xu, Z. Chen, and J. Yang, “Nonlinear spectrum reshaping and gap-soliton-train trapping in optically induced photonic structures”, *Phys. Rev. Lett.* 98, 213903 (2007).
- [13] X. Wang, Z. Chen, J. Wang and J. Yang, “Observation of in-band lattice solitons”, *Phys. Rev. Lett.* 99, 243901 (2007).
- [14] J. Yang, “Transversely stable soliton trains in photonic lattices”, *Phys. Rev. A.* 84, 033840 (2011).
- [15] D.E. Pelinovsky and J. Yang, “On transverse stability of discrete line solitons”, arXiv:1210.0938 [nlin.PS] (2012).
- [16] T. S. Yang and T. R. Akylas, “On asymmetric gravity-capillary solitary waves”, *J. Fluid Mech.* 330, 215–232 (1997).
- [17] L.P. Pitaevskii and S. Stringari, *BoseEinstein Condensation* (Oxford University Press, Oxford, 2003).
- [18] D. E. Pelinovsky, A. A. Sukhorukov, and Y. S. Kivshar, “Bifurcations and stability of gap solitons in periodic potentials”, *Phys. Rev. E* 70, 036618 (2004).
- [19] D. C. Calvo, T. S. Yang, and T. R. Akylas, “On the stability of solitary waves with decaying oscillatory tails”, *Proc. R. Soc. London A* 456, 469–487 (2000).
- [20] J. P. Boyd, *Weakly Nonlocal Solitary Waves and Beyond-All-Orders Asymptotics* (Kluwer, Boston, 1998).
- [21] Y. Pomeau, A. Ramani, and B. Grammaticos, “Structural stability of the Korteweg-de Vries solitons under a singular perturbation,” *Physica D* 31, 127–134 (1988).
- [22] T.R. Akylas and R.H.J. Grimshaw, “Solitary internal waves with oscillatory tails,” *J. Fluid Mech.* 242, 279-298 (1992).
- [23] T.R. Akylas and T.S. Yang, “On short-scale oscillatory tails of long-wave disturbances,” *Stud. Appl. Math.* 94, 1-20 (1995).
- [24] R. Grimshaw and N. Joshi, “Weakly nonlocal solitary waves in a singularly perturbed Kortewegde Vries equation,” *SIAM J. Appl. Math.* 55, 124-135 (1995).

- [25] R. Grimshaw, “Weakly nonlocal solitary waves in a singularly perturbed nonlinear Schrödinger equation,” *Stud. Appl. Math.* 94, 257-270 (1995).
- [26] D.C. Calvo and T.R. Akylas, “On the formation of bound states by interacting nonlocal solitary waves,” *Physica D* 101, 270-288 (1997).
- [27] Z. Shi and J. Yang, “Solitary waves bifurcated from Bloch-band edges in two-dimensional periodic media”, *Phys. Rev. E* 75, 056602 (2007).